Robust quantum anomalous Hall effect with tunable magnetization directions and Chern numbers

Xinming Wu, Runhan Li, Xiaorong Zou, Baibiao Huang, Ying Dai,* and Chengwang Niu†
School of Physics, State Key Laboratory of Crystal Materials, Shandong University, Jinan 250100, China

(Received 8 July 2023; revised 12 September 2023; accepted 19 September 2023; published 29 September 2023)

The quantum anomalous Hall effect (QAHE) has attracted significant attention as it provides intriguing platforms for exploring prominent physical phenomena and applications of low-dissipation devices. Here, we put forward that, unlike previously reported QAH insulators emerging with either out-of-plane or in-plane magnetizations, robust QAHE can be obtained in a two-dimensional ferromagnet regardless of the magnetization directions. In particular, we identify the intrinsic ferromagnetic $NiBiO_3$ as a feasible candidate material with the nontrivial topology explicitly confirmed by nonzero integer Chern numbers $\mathcal{C}$ and the emergence of chiral edge states. Moreover, we proclaim that the Chern numbers can be tuned and a high-Chern-number QAHE, characterized by $\mathcal{C} = \pm 3$, is obtained by tuning the magnetization from the in-plane to out-of-plane direction. Our findings not only advance the general understanding of QAHE but also put forward potential applications in topotronics.

DOI: 10.1103/PhysRevB.108.115438

I. INTRODUCTION

The quantum anomalous Hall effect (QAHE) has garnered considerable attention as a fascinating milestone of magnetic topological states [1–4]. As is well known, QAHE, a zero-magnetic-field quantum Hall effect arising in the presence of spontaneous magnetization, is characterized by quantized anomalous Hall conductance $\sigma_{xy} = \mathcal{C}e^2/h$, where $\mathcal{C}$ is the Chern number, and dissipationless chiral edge states [5]. QAHE provides a versatile playground for investigating emerging quantum phenomena such as topological magnetoelectric effects, Majorana fermions, and so on [6–9]. Moreover, the chiral edge states of QAHE can conduct without dissipation, which is pivotal for the innovative design of low-power-consumption spintronic devices [1–4]. Indeed, QAHE is currently maturing into a significantly burgeoning research field and numerous candidates have been theoretically proposed to host the QAHE [10–21]. Experimentally, successful achievements of QAHE are Cr-doped $(Bi, Sb)_2Te_3$ and intrinsic $MnBi_2Te_4$, but magnetic inhomogeneity limits the observation temperature for Cr-doped $(Bi, Sb)_2Te_3$ and an external magnetic field is needed to drive the magnetization direction to out of plane for $MnBi_2Te_4$ [22–26]. In addition, the research on QAHE has recently started to reach out to in-plane ferromagnetism when all the mirror symmetries are broken, such as in group-V elements with a buckled honeycomb lattice and single-layer (SL) LaCl [27–30]. Despite being actively explored, the QAHE that is robust against magnetization directions remains elusive, and it would be of great significance to obtain it in intrinsic two-dimensional (2D) magnets.

It is well known that the Chern number $\mathcal{C}$ corresponds to the circulation direction and number of chiral edge states [31,32]. Thus, the direction and number of nondissipative current channels, the landmark features of QAHE, can be controlled by the switching of $\mathcal{C}$. The tuning of the edge current chirality facilitates potential applications of chiral logic devices, and more dissipationless chiral edge channels can significantly improve the performance of QAHE-based devices [33–36]. In fact, the Chern number $\mathcal{C}$ is usually associated with the magnetic doping concentration, structural distortion, and thickness of the thin films, as previously predicted in magnetically doped topological insulators [37–39] and $HgCr_2Se_4$ thin films [40]. In experiment, by increasing the thin film thickness, a high-Chern-number QAHE has been recently realized in $MnBi_2Te_4$ [24] and a multilayer structure of alternating magnetic and undoped topological insulators [41]. However, the Chern number is nonadjustable after generating a material with fixed magnetic doping concentration and/or thickness. Thus, candidates with flexible and controllable tuning of Chern numbers are in high demand for future applications of QAHE.

In the present paper, we theoretically demonstrate that the transition metal oxide $NiBiO_3$ is a prominent QAH insulator with a stable crystal structure and intrinsic ferromagnetic (FM) coupling. Remarkably, in contrast to previously proposed ones, the QAHE in SL $NiBiO_3$ can be obtained under various magnetization directions, including in-plane, out-of-plane, and canted FM configurations. For in-plane magnetization that breaks all mirror symmetries, QAHE emerges with the calculations of the anomalous Hall conductance σ_{xy}, Wannier charge centers, and edge states confirming the nontrivial topology. By tuning the direction of in-plane magnetization, the chirality of QAHE can be periodically switched with alternative Chern numbers of $\mathcal{C} = \pm 1$, and a Weyl-like semimetal is obtained when the magnetization is perpendicular to the mirror planes. Remarkably, while the

*daiy60@sdu.edu.cn
†c.niu@sdu.edu.cn

 ©2023 American Physical Society

QAHE phase remains intact, we show that the Chern numbers can be tuned and increased to $\mathcal{C} = \pm 3$ by tuning the magnetization to the out-of-plane directions. Our findings pave a way to the utilization of QAHE as seed materials for arriving at robust topologically nontrivial phases.

II. COMPUTATIONAL DETAILS

We use the Vienna *ab initio* simulation package (VASP) [42] to perform first-principles calculations on the basis of density functional theory. The generalized gradient approximation (GGA) of Perdew-Burke-Ernzerhof (PBE) is used for the exchange-correlation potential [43]. The cutoff energy is fixed to 500 eV, and all structures are relaxed until the residual forces are less than 0.01 eV/Å. We use a 15-Å vacuum layer to avoid interactions between nearest slabs. The GGA + U method with a value of $U = 3$ eV for Ni-d electrons is used to correct the Coulomb interaction [44]. Maximally localized Wannier functions (MLWFs), combining the results of first-principles calculations of VASP, are constructed in the basis of O/Bi-p and Ni-d orbitals by using the WANNIER90 code [45]. The phonon calculations are carried out using the PHONOPY code [46].

III. RESULTS AND DISCUSSION

Single-layer (SL) $NiBiO_3$ crystallizes in a hexagonal lattice with space group $P\bar{3}1m$, stacking in a sequence of Bi-O-Ni-O-Bi, as depicted in Fig. 1(a). There are ten atoms in the unit cell of SL $NiBiO_3$, where six O atoms occupy the Wyckoff 6k position, two Ni atoms occupy the 2d position, and two Bi atoms occupy the 2e position. The optimized lattice constant is $a = 5.09$ Å, and Bi-O and Ni-O bond lengths are 2.12 and 1.95 Å, respectively. The formation energy of SL $NiBiO_3$ is computed as the energy difference between SL $NiBiO_3$ and the Ni, Bi crystal, and oxygen molecule, given by $E_{\text{form}} = E_{\text{NiBiO}_3} - E_{\text{Ni}} - E_{\text{Bi}} - 3/2\,E_{\text{O}_2}$. The obtained formation energy of -3.01 eV implies that the SL $NiBiO_3$ is energetically stable and its experimental synthesis is achievable. The dynamical stability is investigated via the phonon spectrum calculations. As illustrated in Fig. 1(c), there is no imaginary frequency in the entire Brillouin zone, revealing that the SL $NiBiO_3$ is dynamically stable. Moreover, molecular dynamics simulations are carried out for 10 ps at 300 K. As illustrated in Fig. 1(d), there is neither bond breakage nor structure reconstruction, suggesting a robust thermal stability for SL $NiBiO_3$.

To determine the magnetic ground state of SL $NiBiO_3$, we considered nonmagnetic, ferromagnetic, and antiferromagnetic configurations. The energy gain resulting from spin polarization is about 0.31 eV per Ni, meaning that the ground state of SL $NiBiO_3$ is spin polarized. Our spin-polarized total energy calculations indicate that the FM state is energetically favored over the antiferromagnetic (AFM) one by 91.4 meV per Ni, attributed to the Ni-O-Ni superexchange interactions, and this large value suggests that the FM coupling is strong and robust in the SL $NiBiO_3$. A Ni atom is coordinated by six O atoms with distorted octahedra, and such a local crystal field splits the d shell into three groups: d_{z^2}, (d_{xy}, $d_{x^2-y^2}$), and (d_{xz}, d_{yz}). The calculated 1.0μ_B of net magnetic moment per

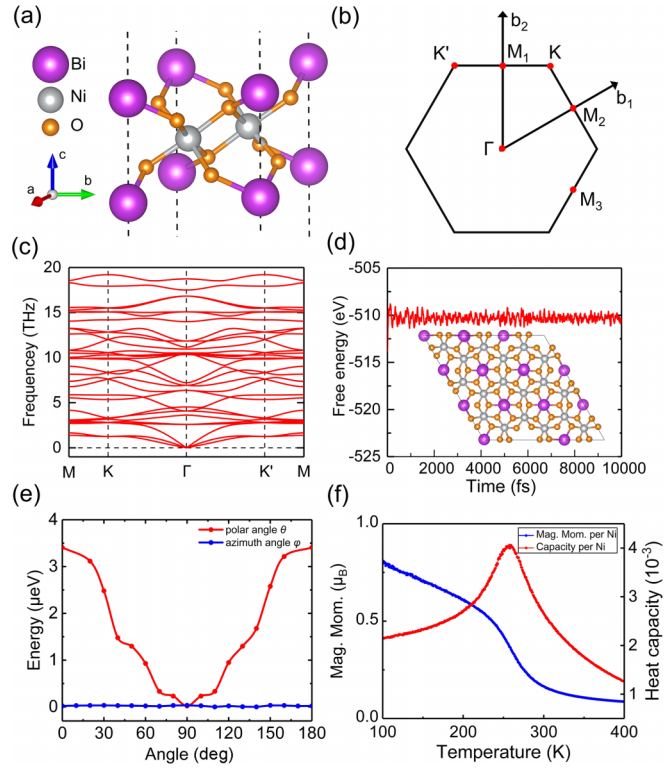

FIG. 1. (a) Crystal structure of single-layer (SL) $NiBiO_3$ in space group $P\bar{3}1m$. (b) The first Brillouin zone with high-symmetry points denoted as red dots. (c) The phonon dispersion and (d) time evolution of free energy during the molecular dynamics calculations for SL $NiBiO_3$, showing that the SL is dynamically and thermally stable. (e) Energy differences of SL $NiBiO_3$ with respect to the magnetization directions θ and φ. (f) Temperature variation of the Monte Carlo averaged spin and heat capacity per Ni for SL $NiBiO_3$.

Ni indicates that the Ni atom has a $3d^7$ configuration, which yields a low-spin state, i.e., six electrons occupy the d_{z^2} and (d_{xy}, $d_{x^2-y^2}$) orbitals, and then the remaining one electron fills one of the (d_{xz}, d_{yz}) orbitals. After including the SOC effect, we further study the magnetic anisotropy energy (E_{MAE}) of SL $NiBiO_3$. As shown in Fig. 1(e), the polar angle of $\theta = 90^\circ$ with an in-plane direction corresponds to the minimum E_{MAE}, and the polar angle of $\theta = 0^\circ$ (or $\theta = 180^\circ$) with an out-of-plane direction corresponds to the maximum E_{MAE}. The E_{MAE} exhibits a dependence on the polar angle θ while showing almost identical behavior for different azimuthal angles φ, reaching a small value of $E_{\text{MAE}} = 3.4$ μeV per Ni that may be tuned by an external field. Furthermore, based on the Heisenberg Hamiltonian, the Curie temperature of SL $NiBiO_3$ was estimated from Monte Carlo simulations to be as large as 258 K [47], revealing the possibility of potential applications at high temperature.

Figure 2(a) presents the spin-polarized band structures in the absence of SOC, where the red and blue bands correspond to the spin-up and spin-down channels, respectively. Because of intrinsic spin polarization, the bands of opposite spins are clearly split far away from each other. While a gap appears in the spin-down bands, the spin-up bands that are left around the Fermi level are gapless with the Weyl-like band crossings along Γ-M, revealing a good half-metallic characteristic

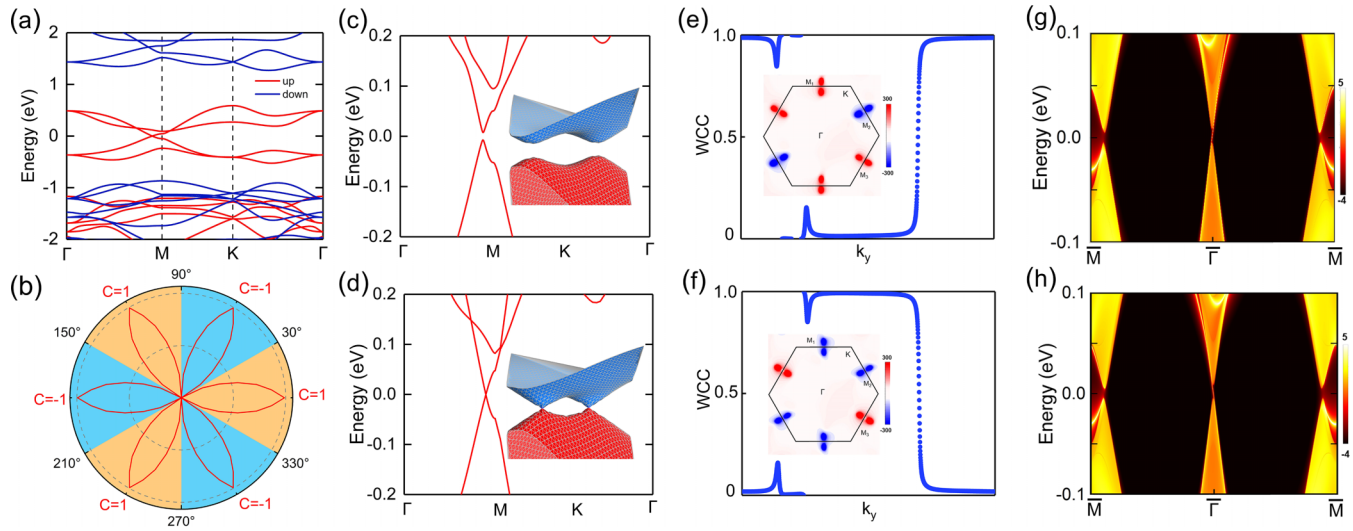

FIG. 2. (a) Band structures of SL $NiBiO_3$ without spin-orbit coupling (SOC). The spin-up bands are gapless while a gap emerges in the spin-down bands. (b) Phase diagram of energy gaps and Chern numbers vs the azimuthal angle φ for in-plane magnetization. The radial value of the red line represents the magnitude of the corresponding band gap. Band structures of SL $NiBiO_3$ with SOC for the in-plane magnetization with (c) breaking and (d) preserving the mirror symmetry at $\varphi = 0^\circ$ and $\varphi = 30^\circ$, respectively. Insets are the corresponding three-dimensional (3D) band structures around the M points. Evolution of the sum of Wannier charge centers for SL $NiBiO_3$ with (e) $\varphi = 0^\circ$ and (f) $\varphi = 60^\circ$, showing the QAHE with opposite Chern numbers of $\mathcal{C} = -1$ and $\mathcal{C} = 1$, respectively. Insets present the reciprocal-space distribution of Berry curvatures for all occupied bands. Energy dispersions of a semi-infinite $NiBiO_3$ nanoribbon with (g) $\varphi = 0^\circ$ and (h) $\varphi = 60^\circ$ confirm the topological nature with opposite chirality.

near the Fermi energy. Remarkably, taking SOC into account, the electronic and topological properties are highly sensitive to the orientations of ferromagnetization. As illustrated in Figs. 1(a) and 1(b), there are three mirror planes in SL $NiBiO_3$ along the Γ-K (K') lines. One of the three mirror planes survives when the in-plane ferromagnetization is perpendicular to it, and consequently the system still remains gapless and shows a half-metallic character. If the in-plane ferromagnetization breaks all mirror symmetries, as depicted in Fig. 2(c), a global gap of 1.5 meV opens at the Weyl-like point when the in-plane ferromagnetization is not perpendicular to any of the three mirror planes.

To confirm the topologically nontrivial character of the gap, we calculate the Chern number $\mathcal{C}$, given by $\mathcal{C} = \frac{1}{2\pi}\int_{\mathrm{BZ}} \Omega(\mathbf{k}) d^2k$. Here, $\Omega(\mathbf{k})$ is the Berry curvature over all of the occupied states [48,49],

$$\Omega(\mathbf{k}) = -\sum_{n<E_F}\sum_{m\neq n} 2\,\mathrm{Im}\frac{\langle\psi_{n\mathbf{k}}|\upsilon_x|\psi_{m\mathbf{k}}\rangle\langle\psi_{m\mathbf{k}}|\upsilon_y|\psi_{n\mathbf{k}}\rangle}{(\varepsilon_{m\mathbf{k}}-\varepsilon_{n\mathbf{k}})^2}, \quad (1)$$

where m, n are band indices, and $\psi_{m/n\mathbf{k}}$ and $\varepsilon_{m/n\mathbf{k}}$ represent the Bloch wave functions and corresponding eigenenergies of band m/n, respectively. $\upsilon_{x/y}$ are the velocity operators. As expected, arising mainly from the Berry curvature $\Omega(\mathbf{k})$ around the M points as shown in Fig. 2(e), the Chern number indeed acquires an integer value of $\mathcal{C} = 1$. We then employ the Wilson loop method to confirm the nonzero Chern number $\mathcal{C}$ as displayed in Fig. 2(e), demonstrating the QAH effect in SL $NiBiO_3$ even with in-plane ferromagnetization.

The existence of chiral edge states is one of the most important properties of the QAH effect. The integer value of $\mathcal{C} = 1$ indicates that there is one gapless edge state in the nontrivial gap for SL $NiBiO_3$. To illustrate this, we carry out calculations of the edge states using the MLWFs of SL $NiBiO_3$, and the results for its semi-infinite nanoribbon are displayed in Fig. 2(g). One can clearly see one chiral edge state around the Γ point. This is in direct agreement with the calculated Chern number $\mathcal{C} = 1$, and further explicitly confirms the QAH state in SL $NiBiO_3$.

We then rotate the magnetic directions, which provides a promising way to control both symmetry and topology. There are two cases that need to be considered, namely, the polar angle θ indicates the directions between in plane and out of plane, and the azimuth angle φ represents the in-plane magnetization with different directions. While the energy difference is negligible, where, as displayed in Fig. 1(e), with E_{MAE} it is almost zero, we start by considering the situations of in-plane magnetization with different φ. Indeed, switching the angle φ can result in a gap closure and give rise to a nontrivial semimetallic state when the in-plane magnetization is perpendicular to the mirror planes. If φ exceeds the critical values, the reopening of the energy gap is obtained.

Figure 2(d) indicates that there are two isolated band crossing points along the Γ-M line when the mirror symmetry survives, and remarkably the two band crossing points mediate the topological phase transitions from the nontrivial Chern numbers $\mathcal{C} = 1$ to $\mathcal{C} = -1$, and/or vice versa. The band structures appear to be quite similar to that of $\mathcal{C} = 1$. However, the signs of the Berry curvatures are different. One can find that two-thirds of the Berry curvatures are positive while they are negative in the remaining one-third parts for $\mathcal{C} = 1$. In contrast, for $\mathcal{C} = -1$, two-thirds are negative and one-third is positive. The opposite chirality is further explicitly confirmed by the Wannier charge center (WCC) calculations and the gapless edge states that reverse their propagating directions

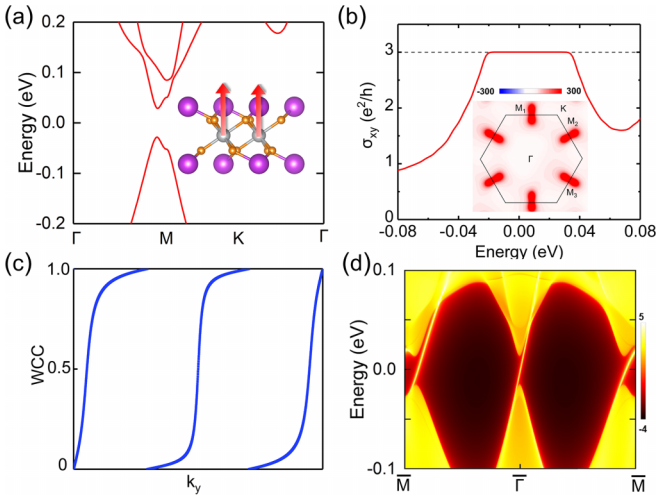

FIG. 3. (a) Band structures of SL $NiBiO_3$ with SOC for out-of-plane magnetization. (b) Energy dependence of the anomalous Hall conductivity σ_{xy}, revealing a quantized value within the energy window of the SOC gap. The inset shows the reciprocal-space distribution of Berry curvatures within the SOC gap. (c) Evolution of the sum of WCCs for all occupied states suggests a high Chern number of $\mathcal{C} = 3$. (d) Energy dispersion of a semi-infinite ribbon shows three chiral edge states within the SOC gap.

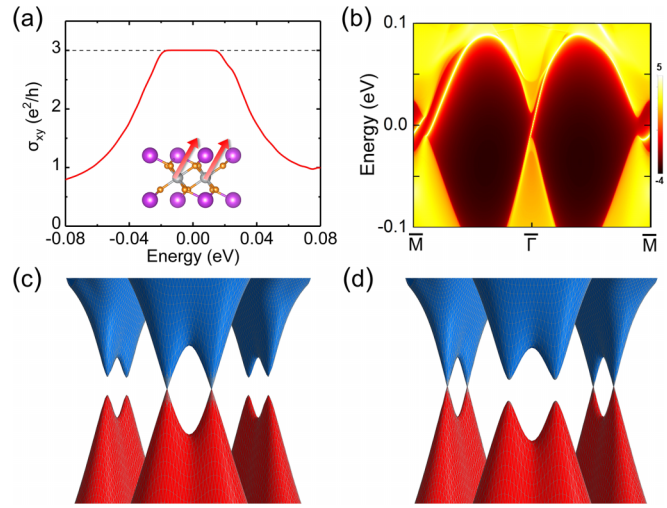

FIG. 4. (a) The anomalous Hall conductivity σ_{xy} and (b) energy dispersion of a semi-infinite ribbon for SL $NiBiO_3$ with polar angle $\theta = 30^\circ$. (c) 3D band structures of SL $NiBiO_3$ with (c) $\theta = 66.8^\circ$, $\varphi = 0^\circ$ and (d) $\theta = 77.3^\circ$, $\varphi = 180^\circ$.

as shown in Figs. 2(f) and 2(h). There are three mirror planes in SL $NiBiO_3$ and thus the band gap closing emerges in the interval of 60°. Consequently, there is a periodic jumping of the QAH states with alternative Chern numbers $\mathcal{C} = \pm 1$ in the interval of 60° as illustrated in Fig. 2(b). Similar to a previous study [50], we found that the band gap value of SL $NiBiO_3$ is contingent upon the extent of symmetry breaking and can be precisely characterized by a sine function. The global band gap exhibits periodic variations with changes in the magnetic direction.

Another distinctive type of magnetic direction is the out-of-plane direction, which breaks all three of the above-mentioned mirror planes. As presented in Fig. 3(a), a direct-gap insulator with an energy gap of 5.7 meV is obtained. To gain insights into the topological characters in this case, the anomalous Hall conductivity σ_{xy} is calculated and presented versus the position of the Fermi level in Fig. 3(b). The quantization of σ_{xy} with an integer value of $\mathcal{C} = 3$, when the Fermi level is located within the energy gap, is clearly visible. Remarkably, there are three chiral edge states within the nontrivial band gap, as shown in Fig. 3(d), confirming the nontrivial QAH effect in SL $NiBiO_3$ and thus that a phase transition from low $\mathcal{C}$ to high $\mathcal{C}$ can be effectively tuned by the magnetic directions. To elucidate this transition more clearly, we present the 2D distribution of Berry curvatures in the inset of Fig. 3(b). Different from the QAH state with $\mathcal{C} = 1$, we see that the nonzero Berry curvatures $\Omega(\mathbf{k})$ are localized around the M points with the same sign, and the evolution of WCCs with winding number 3 corroborates the nontrivial Chern numbers $\mathcal{C} = 3$.

We further consider the case of canted magnetizations and discuss the characteristics of the band structures when transitioning between different Chern numbers. Taking $\theta = 30^\circ$ as an example, Figs. 4(a) and 4(b) indicate that the QAH state with $\mathcal{C} = 3$ remains intact for SL $NiBiO_3$ with canted magnetizations. The global band gap decreases with increasing polar angle θ, and indeed the band gap undergoes a closing and reopening process, suggesting a topological phase transition. However, remarkably, the QAHE survives with $\mathcal{C} = \pm 1$, i.e., the QAHE is robust against the magnetization directions with a switchable Chern number. The changes of Chern numbers are different, which are $\Delta\mathcal{C} = 2$ and $\Delta\mathcal{C} = 4$, since the periodic jumping of Chern numbers $\mathcal{C} = \pm 1$ along different φ. To uncover the nontrivial topology of the variation, we exemplified in Figs. 4(c) and 4(d) the 3D band structures with a closed gap for the transitions from $\mathcal{C} = 3$ to $\mathcal{C} = 1$ and $\mathcal{C} = -1$, respectively. In fact, along different φ, the gap closes at different polar angles θ, which are respectively $\theta = 66.8^\circ$ and $\theta = 77.3^\circ$, and the so-called mixed Weyl points are obtained under these critical θ [51]. The numbers of mixed Weyl points amount to the corresponding changes of Chern numbers. This is in direct agreement with the fact that each Weyl point carries a topological charge of 1, whereby it mediates the transitions of QAHE from $\mathcal{C} = 3$ to $\mathcal{C} = 1$ and $\mathcal{C} = -1$.

IV. CONCLUSIONS

In summary, we demonstrated that the 2D stable transition metal oxide of SL $NiBiO_3$ can exhibit an intrinsic QAHE with in-plane magnetization, characterized by a nonzero Chern number $\mathcal{C} = \pm 1$ and a dissipationless chiral edge state. Remarkably, we uncover that, unlike previous configurations where the QAHE may be heavily deformed by tuning the magnetization directions, the QAHE in SL $NiBiO_3$ remains intact with either canted or out-of-plane magnetizations. In particular, the Chern number is tunable, reaching as much as $\mathcal{C} = \pm 3$, and that the long-awaited high-Chern-number QAH state is obtained with the emergence of three chiral edge states. Our results provide an ideal platform to achieve a Chern number tunable QAHE in the same material, which is expected to draw great experimental attention.

ACKNOWLEDGMENTS

This work was supported by the National Natural Science Foundation of China (Grants No. 12174220 and No. 12074217), the Shandong Provincial Key Research and Development Program (Major Scientific and Technological Innovation Project) (Grant No. 2019JZZY010302), and the Qilu Young Scholar Program of Shandong University.

[1] C.-Z. Chang, C.-X. Liu, and A. H. MacDonald, Rev. Mod. Phys. **95**, 011002 (2023).

[2] H. Weng, R. Yu, X. Hu, X. Dai, and Z. Fang, Adv. Phys. **64**, 227 (2015).

[3] Y. Ren, Z. Qiao, and Q. Niu, Rep. Prog. Phys. **79**, 066501 (2016).

[4] C.-X. Liu, S.-C. Zhang, and X.-L. Qi, Annu. Rev. Condens. Matter Phys. **7**, 301 (2016).

[5] F. D. M. Haldane, Phys. Rev. Lett. **61**, 2015 (1988).

[6] J. Zhu, J.-J. Su, and A. H. MacDonald, Phys. Rev. Lett. **125**, 227702 (2020).

[7] X.-L. Qi, T. L. Hughes, and S.-C. Zhang, Phys. Rev. B **82**, 184516 (2010).

[8] D. Xiao, J. Jiang, J.-H. Shin, W. Wang, F. Wang, Y.-F. Zhao, C. Liu, W. Wu, M. H. W. Chan, N. Samarth, and C.-Z. Chang, Phys. Rev. Lett. **120**, 056801 (2018).

[9] C. Niu, N. Mao, X. Hu, B. Huang, and Y. Dai, Phys. Rev. B **99**, 235119 (2019).

[10] R. Yu, W. Zhang, H.-J. Zhang, S.-C. Zhang, X. Dai, and Z. Fang, Science **329**, 61 (2010).

[11] H. Zhang, C. Lazo, S. Blügel, S. Heinze, and Y. Mokrousov, Phys. Rev. Lett. **108**, 056802 (2012).

[12] H. Zhang, Y. Xu, J. Wang, K. Chang, and S.-C. Zhang, Phys. Rev. Lett. **112**, 216803 (2014).

[13] S.-C. Wu, G. Shan, and B. Yan, Phys. Rev. Lett. **113**, 256401 (2014).

[14] Z. Qiao, W. Ren, H. Chen, L. Bellaiche, Z. Zhang, A. H. MacDonald, and Q. Niu, Phys. Rev. Lett. **112**, 116404 (2014).

[15] C. Niu, G. Bihlmayer, H. Zhang, D. Wortmann, S. Blügel, and Y. Mokrousov, Phys. Rev. B **91**, 041303(R) (2015).

[16] G. Xu, J. Wang, C. Felser, X.-L. Qi, and S.-C. Zhang, Nano Lett. **15**, 2019 (2015).

[17] J. Zhou, Q. Sun, and P. Jena, Phys. Rev. Lett. **119**, 046403 (2017).

[18] Z. F. Wang, Z. Liu, J. Yang, and F. Liu, Phys. Rev. Lett. **120**, 156406 (2018).

[19] H. Sun, B. Xia, Z. Chen, Y. Zhang, P. Liu, Q. Yao, H. Tang, Y. Zhao, H. Xu, and Q. Liu, Phys. Rev. Lett. **123**, 096401 (2019).

[20] M. M. Otrokov, I. P. Rusinov, M. Blanco-Rey, M. Hoffmann, A. Y. Vyazovskaya, S. V. Eremeev, A. Ernst, P. M. Echenique, A. Arnau, and E. V. Chulkov, Phys. Rev. Lett. **122**, 107202 (2019).

[21] Y. Li, J. Li, Y. Li, M. Ye, F. Zheng, Z. Zhang, J. Fu, W. Duan, and Y. Xu, Phys. Rev. Lett. **125**, 086401 (2020).

[22] C.-Z. Chang, J. Zhang, X. Feng, J. Shen, Z. Zhang, M. Guo, K. Li, Y. Ou, P. Wei, L.-L. Wang, Z.-Q. Ji, Y. Feng, S. Ji, X. Chen, J. Jia, X. Dai, Z. Fang, S.-C. Zhang, K. He, Y. Wang *et al.*, Science **340**, 167 (2013).

[23] Y. Deng, Y. Yu, M. Z. Shi, Z. Guo, Z. Xu, J. Wang, X. H. Chen, and Y. Zhang, Science **367**, 895 (2020).

[24] J. Ge, Y. Liu, J. Li, H. Li, T. Luo, Y. Wu, Y. Xu, and J. Wang, Natl. Sci. Rev. **7**, 1280 (2020).

[25] C. Liu, Y. Wang, H. Li, Y. Wu, Y. Li, J. Li, K. He, Y. Xu, J. Zhang, and Y. Wang, Nat. Mater. **19**, 522 (2020).

[26] P. M. Sass, W. Ge, J. Yan, D. Obeysekera, J. J. Yang, and W. Wu, Nano Lett. **20**, 2609 (2020).

[27] X. Liu, H.-C. Hsu, and C.-X. Liu, Phys. Rev. Lett. **111**, 086802 (2013).

[28] Y. Ren, J. Zeng, X. Deng, F. Yang, H. Pan, and Z. Qiao, Phys. Rev. B **94**, 085411 (2016).

[29] P. Zhong, Y. Ren, Y. Han, L. Zhang, and Z. Qiao, Phys. Rev. B **96**, 241103(R) (2017).

[30] Z. Liu, G. Zhao, B. Liu, Z. F. Wang, J. Yang, and F. Liu, Phys. Rev. Lett. **121**, 246401 (2018).

[31] C.-Z. Chang, W. Zhao, D. Y. Kim, P. Wei, J. K. Jain, C. Liu, M. H. W. Chan, and J. S. Moodera, Phys. Rev. Lett. **115**, 057206 (2015).

[32] Z. Li, Y. Han, and Z. Qiao, Phys. Rev. Lett. **129**, 036801 (2022).

[33] R.-X. Zhang, H.-C. Hsu, and C.-X. Liu, Phys. Rev. B **93**, 235315 (2016).

[34] L.-J. Zhou, R. Mei, Y.-F. Zhao, R. Zhang, D. Zhuo, Z.-J. Yan, W. Yuan, M. Kayyalha, M. H. W. Chan, C.-X. Liu, and C.-Z. Chang, Phys. Rev. Lett. **130**, 086201 (2023).

[35] H.-Z. Lu, Natl. Sci. Rev. **6**, 208 (2019).

[36] G. Jiang, Y. Feng, W. Wu, S. Li, Y. Bai, Y. Li, Q. Zhang, L. Gu, X. Feng, D. Zhang, C. Song, L. Wang, W. Li, X.-C. Ma, Q.-K. Xue, Y. Wang, and K. He, Chin. Phys. Lett. **35**, 076802 (2018).

[37] J. Wang, B. Lian, H. Zhang, Y. Xu, and S.-C. Zhang, Phys. Rev. Lett. **111**, 136801 (2013).

[38] H. Jiang, Z. Qiao, H. Liu, and Q. Niu, Phys. Rev. B **85**, 045445 (2012).

[39] C. Fang, M. J. Gilbert, and B. A. Bernevig, Phys. Rev. Lett. **112**, 046801 (2014).

[40] G. Xu, H. Weng, Z. Wang, X. Dai, and Z. Fang, Phys. Rev. Lett. **107**, 186806 (2011).

[41] Y.-F. Zhao, R. Zhang, R. Mei, L.-J. Zhou, H. Yi, Y.-Q. Zhang, J. Yu, R. Xiao, K. Wang, N. Samarth *et al.*, Nature (London) **588**, 419 (2020).

[42] G. Kresse and J. Furthmüller, Phys. Rev. B **54**, 11169 (1996).

[43] J. P. Perdew, K. Burke, and M. Ernzerhof, Phys. Rev. Lett. **77**, 3865 (1996).

[44] S. L. Dudarev, G. A. Botton, S. Y. Savrasov, C. J. Humphreys, and A. P. Sutton, Phys. Rev. B **57**, 1505 (1998).

[45] A. A. Mostofi, J. R. Yates, Y.-S. Lee, I. Souza, D. Vanderbilt, and N. Marzari, Comput. Phys. Commun. **178**, 685 (2008).

[46] A. Togo and I. Tanaka, Scr. Mater. **108**, 1 (2015).

[47] See Supplemental Material at http://link.aps.org/supplemental/10.1103/PhysRevB.108.115438 for complete Monte Carlo simulations, and phase diagrams of energy gaps and Chern numbers versus the polar angle and orbitally resolved band structures.

[48] D. J. Thouless, M. Kohmoto, M. P. Nightingale, and M. den Nijs, Phys. Rev. Lett. **49**, 405 (1982).

[49] Y. Yao and Z. Fang, Phys. Rev. Lett. **95**, 156601 (2005).

[50] Y. Yu, X. Chen, X. Liu, J. Li, B. Sanyal, X. Kong, F. M. Peeters, and L. Li, Phys. Rev. B **105**, 024407 (2022).

[51] C. Niu, J.-P. Hanke, P. M. Buhl, H. Zhang, L. Plucinski, D. Wortmann, S. Blügel, G. Bihlmayer, and Y. Mokrousov, Nat. Commun. **10**, 3179 (2019).